

Investigating the parity of the exotic Θ^+ baryon from kaon photoproduction

Byung Geel Yu,^{1,2,*} Tae Keun Choi,^{3,†} and Chueng-Ryong Ji^{2,‡}

¹*Department of General studies, Hangkong Aviation University, Koyang, 200-1, Korea*

²*Department of Physics, North Carolina State University,
Raleigh, North Carolina 27695-8202, USA*

³*Department of Physics, Yonsei University, Wonju, 220-710, Korea*

(Dated: November 1, 2018)

Abstract

Based on the hadronic model with the gauge prescription suggested by Ohta and Haberzettl, we investigate the possibility of determining the parity state of the Θ^+ baryon using photon induced processes, $\gamma n \rightarrow K^- \Theta^+$ and $\gamma p \rightarrow \bar{K}^0 \Theta^+$. The total and differential cross sections are simulated in two versions of pseudovector(PV) and pseudoscalar(PS) coupling schemes and the results are reported both on the positive and negative parity states of the Θ^+ baryon. It is found that in both coupling schemes the total cross sections from the neutron target are in general larger than those from the proton target, regardless of the Θ^+ parities. The cross sections of the Θ^+ production however depend largely on the value of the Θ^+ decay width which is not yet well established. Moreover, there is a wide theoretical uncertainty associated with the different assumption on the gauge prescription in model calculations. We discuss these points by comparing theoretical predictions with the existing experimental data. Our analysis suggests that the observation of the angular distribution rather than just the total cross section in the photoproduction process may be a useful tool to distinguish the parity of the Θ^+ baryon.

PACS numbers: 13.60.Rj,13.60.-r,13.75.Jz,14.20.-c

*Electronic address: bgyu@mail.hankong.ac.kr

†Electronic address: tkchoi@dragon.yonsei.ac.kr

‡Electronic address: crji@unity.ncsu.edu

I. INTRODUCTION

The recent experimental observations of the narrow baryon state from the invariant mass spectrum of K^+n or K^0p in photon induced nuclear reactions and their interpretation as an exotic pentaquark state of the Θ^+ baryon with $s=+1$ attracted a lot of attention [1, 2, 3, 4, 5]. Such an experimental evidence for the Θ^+ baryon was also observed in other reaction channels, $K^+Xe \rightarrow K^0pXe'$ [6], $\nu_{\mu^-}(\bar{\nu}_{\mu^-})$ collisions with nuclei [7] and $pA \rightarrow pK_s^0X$ [8], which tend to confirm the existence of the Θ^+ baryon. The extracted mass of the Θ^+ baryon from these experiments is reported to be 1.54 GeV and its decay width less than 25 MeV are consistent with those of the pentaquark state predicted in the chiral soliton model [9, 10, 11, 12].

These experimental identifications of the Θ^+ have initiated intensive studies of the new type of hadron structures that are containing more than two or three quarks [13, 14]. However, since quantum numbers other than its mass and decay width of the detected Θ^+ baryon are not yet known from these experiments, much theoretical attention has been paid to the determination of its further properties like spin, isospin, parity and its magnetic moment. Subsequent theoretical investigations on the structure of the Θ^+ baryon follow based on the constituent quark model including diquark-diquark- \bar{q} approach [15, 16, 17, 18, 19, 20, 21], Skyrme model [10, 11, 12, 22, 23, 24, 25, 26], QCD sum rule [27, 28, 29], chiral potential model [30], large N_c QCD [31], lattice QCD [32, 33] and Group theory approach [34, 35]. The dynamical properties of the Θ^+ baryon was also studied through the production of the Θ^+ in the relativistic nuclear collisions [36, 37].

All these theoretical studies address various aspects of the Θ^+ baryon properties and in many cases the models assume or predict a definite parity for the Θ^+ as positive [9, 16, 17, 18, 20, 21, 24, 28, 30]. However, recent works from the QCD-sum rules [27, 29] and the lattice QCD [32, 33] favor a negative parity. Therefore the assumptions on or the model predictions for the parity of the Θ^+ are still controversial and it is thus of importance to analyze the processes that may reveal the true parity state of the Θ^+ .

Along this line of thoughts, there are theoretical attempts to determine the parity of the Θ^+ baryon by the direct estimation of the cross sections observed in the photon and meson induced Θ^+ production experiments using hadronic models [38, 39, 41, 42, 43]. In particular, the cross sections of $\gamma n \rightarrow K^-\Theta^+$ and $\gamma p \rightarrow \bar{K}^0\Theta^+$ have been estimated with the hadronic models including hadron form factors [39, 41] and compared with the data from the SAPHIR experiment [2]. The use of hadron form factors requires, of course, the gauge invariance of the photoproduction amplitude and this constraint is indeed satisfied in Refs. [39, 41]. Yet, in view of the model development

in the similar processes, $\gamma p \rightarrow K^+ \Lambda$ and $\gamma p \rightarrow K^+ \Sigma^0$ [44, 45, 46, 47], the gauge prescription suggested by Ohta [48] and Haberzettl [49] yields the better χ^2 -fit for the analysis of the $\gamma p \rightarrow K^+ \Lambda$ process and has a firm field theoretic foundation. Since this point cannot be overlooked, we apply the prescription of Refs. [48, 49] to the model calculation of the processes $\gamma n \rightarrow K^- \Theta^+$ and $\gamma p \rightarrow \bar{K}^0 \Theta^+$.

To focus on the difference in the gauge prescription from the earlier work, we use the same model parameters of Ref. [41]. While Ref.[41] concluded that the total cross section already determined the parity of the Θ^+ as positive, our results indicate that there is a wide theoretical uncertainty associated with the different assumptions on the gauge prescription and the total cross section itself cannot yield a definite conclusion on the parity of the Θ^+ . We thus stress that further analysis of the angular distributions is necessary. Especially, the features of the angular distribution near threshold become less dependent on the model parameters because they follow the conservation rules of parity and angular momentum.

This paper is organized as follows. In Sec. II, the cross section and the differential cross section for angular distribution are evaluated for the Θ^+ production from $\gamma N \rightarrow K \Theta^+$ when the Θ^+ has the positive parity. The cross section and angular distribution of the reaction in the case of the negative parity Θ^+ production are evaluated in Sec. III. Summary and discussion follow in Sec. IV.

II. PHOTOPRODUCTION FOR THE POSITIVE PARITY Θ^+

The photoproduction of the Θ^+ baryon from neutron or proton target is usually calculated in relativistic hadron models because the models with hadronic degrees of freedom are more relevant than the perturbative QCD to the energy range of the reactions that we study in this work. In hadronic models the reaction is generated from the Feynman diagrams at tree level as shown in Fig. 1. The momenta of the incident photon, the nucleon, the outgoing kaon, and the Θ^+ are k , p , q , and p' , respectively in the diagrams of Fig. 1. The Mandelstam variables are $s = (p + k)^2$, $t = (k - q)^2$, and $u = (p' - k)^2$. Using effective Lagrangians for vertex couplings pertinent to the diagrams, the transition amplitude is obtained. Here, as the interaction Lagrangians relevant to the process are found in many literatures [39, 40, 41, 43] we will not repeat them. Instead, with the interaction Lagrangians given in Refs. [39, 41], let us begin with the Born amplitude for the positive parity Θ^+ photoproduction. The Born amplitude of the PV coupling $KN\Theta^+$ interaction

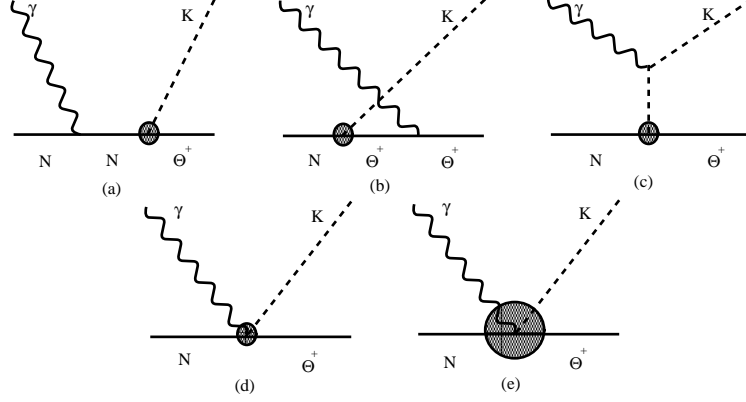


FIG. 1: Tree level diagrams for $\gamma N \rightarrow K\Theta^+$ reaction. Diagrams (a), (b) and (c) denote the s-, u- and t-channel pole terms with hadron form factors depicted as the blob at each vertex. The diagram (d) is the Kroll-Ruderman(KR) term; it is absent for pseudoscalar couplings with bare vertices. The last diagram (e) corresponds to the contact interaction term required to restore gauge invariance of the Born amplitude. It is depicted as a large blob to distinguish from the KR term.

can be written as

$$\mathcal{M}_{Born} = \mathcal{M}_{PV-pole} + \mathcal{M}_{KR} + \mathcal{M}_c. \quad (1)$$

The PV-pole terms are composed of the first three pole diagrams of (a), (b) and (c) in Fig. 1 which correspond to the nucleon, Θ^+ and kaon exchanges in the s-, u- and t-channel respectively, i.e.,

$$\begin{aligned} & \mathcal{M}_{PV-pole} \\ &= \frac{e g_{KN\Theta}}{M + M_\Theta} \bar{u}_\Theta(p') \left\{ F_1(s) \gamma_5 \not{\not{p} + \not{k} + M} \left[Q_N \not{\epsilon} + i \frac{\kappa_N}{2M} \sigma^{\mu\nu} \epsilon_\mu k_\nu \right] + \left[Q_\Theta \not{\epsilon} + i \frac{\kappa_\Theta}{2M_\Theta} \sigma^{\mu\nu} \epsilon_\mu k_\nu \right] \right. \\ & \times \left. \frac{(\not{p}' - \not{k} + M_\Theta)}{u - M_\Theta^2} \gamma_5 \not{\not{p}} F_2(u) + Q_K F_3(t) \gamma_5 (M + M_\Theta) \frac{(2q - k) \cdot \epsilon}{t - m_K^2} \right\} u_N(p). \end{aligned} \quad (2)$$

For brevity, we write the amplitude collectively for $\gamma n \rightarrow K^- \Theta^+$ and $\gamma p \rightarrow \bar{K}^0 \Theta^+$ with notations Q_N , Q_Θ and Q_K by assigning $Q_N = 0$, $Q_\Theta = 1$ and $Q_K = -1$ to $\gamma n \rightarrow K^- \Theta^+$, and $Q_N = 1$, $Q_\Theta = 1$ and $Q_K = 0$ to $\gamma p \rightarrow \bar{K}^0 \Theta^+$, respectively. The anomalous magnetic moments of the proton and neutron are $\kappa_p = 1.79$ and $\kappa_n = -1.91$. In Eq.(2), $g_{KN\Theta}$ is the Θ^+ coupling constant, κ_Θ is the anomalous magnetic moment of Θ^+ , and ϵ is the photon polarization vector. Also, $F_1(s) = F_1(s, M'^2, m_\pi^2)$, $F_2(u) = F_2(M^2, u, m_\pi^2)$ and $F_3(t) = F_3(M^2, M'^2, t)$ are the hadron form factors introduced to the $KN\Theta$ vertices in the s-,u- and t-channel with the normalizations $F_1(s = M^2) = 1$, $F_2(u = M'^2) = 1$ and $F_3(t = m_\pi^2) = 1$, respectively.

In the PV coupling, the Kroll-Ruderman term of Fig. 1 (d) is required to restore gauge invariance

of PV pole terms due to the $\gamma_5 \not{q}$ coupling;

$$\mathcal{M}_{KR} = -\frac{e g_{KN\Theta}}{M + M_\Theta} \bar{u}_\Theta(p') \gamma_5 \not{\epsilon} \left\{ F_1(s) Q_N - Q_\Theta F_2(u) \right\} u_N(p). \quad (3)$$

In the gauge transformation of the PV coupling pole terms together with the Kroll-Ruderman term, however, these amplitudes are not gauge invariant, but yield the following relation,

$$(\mathcal{M}_{PV-pole} + \mathcal{M}_{KR})_{\epsilon \rightarrow k} = e g_{KN\Theta} \bar{u}_\Theta(p') \gamma_5 \left\{ F_1(s) Q_N - Q_\Theta F_2(u) - Q_K F_3(t) \right\} u_N(p). \quad (4)$$

The nonvanishing divergence of Eq.(4) is due to the use of different form factor for each hadron vertex and this sort of divergence equally holds for the gauge transformation of PS coupling photoproduction amplitude. In fact it vanishes when $F_i = 1$ for $i = 1, 2, 3$, i.e., in the case of point interaction of $KN\Theta$, or when $F_i = F$ for all i , i.e., in the case of using an overall form factor, F . In Refs. [39, 41], the recipe they used in order to restore gauge invariance of the Born amplitude as given in Eq.(4) corresponds to the case of using an overall form factor. In this work, we follow the gauge prescription suggested by Ohta [48] and later improved further by Haberzettl [49]. According to these field theoretic analyses [48, 49], the divergence of the hadronic current due to the different form factors can be removed by introducing the diagram (e) of Fig. 1, so called contact interaction term. It is of the form;

$$\begin{aligned} \mathcal{M}_c = & -e g_{KN\Theta} \bar{u}_\Theta(p') \gamma_5 \left\{ (F_1(s) - \widehat{F}) Q_N \frac{(2p+k) \cdot \epsilon}{s - M^2} + Q_\Theta (F_2(u) - \widehat{F}) \frac{(2p' - k) \cdot \epsilon}{u - M_\Theta^2} \right. \\ & \left. + Q_K (F_3(t) - \widehat{F}) \frac{(2q - k) \cdot \epsilon}{t - m_K^2} \right\} u_N(p). \end{aligned} \quad (5)$$

Here, \widehat{F} is a subtraction function which depends on the Mandelstam variables (s, u, t) . Note that in order to maintain the original singularity structure of the Born amplitude, each of the three pole terms in Eq.(5) should be nonsingular, i.e., $\widehat{F} = 1$ for on-mass shell and this can be a constraint on the arbitrary choice of the function \widehat{F} [50, 51]. In this work, to preserve the crossing symmetry of the amplitude, we choose the subtraction function, in specific,

$$\widehat{F} = F_2(u) + F_3(t) - F_2(u)F_3(t), \quad \widehat{F} = F_1(s) + F_2(u) - F_1(s)F_2(u) \quad (6)$$

for $\gamma n \rightarrow K^- \Theta^+$ and $\gamma p \rightarrow \bar{K}^0 \Theta^+$, respectively. For each hadron form factor in the channels $x = s, u, t$, (or $i=1, 2, 3$), we use

$$F_i(x, M_i) = \frac{\Lambda^4}{\Lambda^4 + (x - M_i^2)^2}, \quad (7)$$

which are normalized to unity at $x = M_i^2$. Here M_i is the mass of the exchanged particle and x is the square of the transferred momentum. This function has the correct on-shell condition, i.e., $F_i(x = M_i^2) = 1$ for $i=1, 2, 3$ and, thus, $\widehat{F} = 1$ by Eq.(6).

In the PS coupling, the Born amplitude is composed of those terms depicted by Figs. 1(a) - (c). By the procedure similar to that of PV coupling, the Born amplitude which preserves gauge invariance can be obtained by

$$\mathcal{M}_{Born} = \mathcal{M}_{PS-pole} + \mathcal{M}_c, \quad (8)$$

where

$$\begin{aligned} & \mathcal{M}_{PS-pole} \\ &= e g_{KN\Theta} \bar{u}_\Theta(p') \left\{ F_1(s) \gamma_5 \frac{(\not{p} + \not{k} + M)}{s - M^2} [Q_N \not{\epsilon} + i \frac{\kappa_N}{2M} \sigma^{\mu\nu} \epsilon_\mu k_\nu] + [Q_\Theta \not{\epsilon} + i \frac{\kappa_\Theta}{2M_\Theta} \sigma^{\mu\nu} \epsilon_\mu k_\nu] \right. \\ & \times \left. \frac{(\not{p}' - \not{k} + M_\Theta)}{u - M_\Theta^2} \gamma_5 F_2(u) + Q_K F_3(t) \gamma_5 \frac{(2q - k) \cdot \epsilon}{t - m_K^2} \right\} u_N(p), \quad (9) \end{aligned}$$

and the contact interaction term of Fig. 1 (e) is given by Eq.(5).

In the calculation of cross sections based on this framework, the coupling constant $g_{KN\Theta}$ and the anomalous magnetic moment κ_Θ are to be determined. Unfortunately, there are no detailed informations available on these quantities at present. Instead, we have only few experimental observations; the decay width Γ_Θ and the cross section. It has been reported that the decay width Γ_Θ is measured in the range $9 \sim 25$ MeV [1, 2, 3, 4, 5, 6, 8] and the mean cross section for $\gamma p \rightarrow \bar{K}^0 \Theta^+$ in the SAPHIR experiment is in the order of 200 nb up to $E_\gamma = 2.6$ GeV [2]. More recently HERMES experiment estimated the cross section of the Θ^+ production to be $100 \sim 220$ nb from the quasi-real photoproduction on deuteron, $eD \rightarrow p K_s^0 X$ [5]. However, the precise measurements of the width and cross sections are still lacking and there are on-going discussions about possible reanalyses of these observables [52, 53, 54]. In particular, using the K^+d scattering data, Nussinov reanalyzed the decay width of Θ^+ and came up with $\Gamma_\Theta < 6$ MeV [52]. Moreover, Arndt *et. al.* suggested $\Gamma_\Theta \leq 1$ MeV based on the K^+p and K^+d database [53]. In this work, we adopt $g_{KN\Theta}=2.2$ assuming $\Gamma_\Theta \simeq 5$ MeV for the positive parity Θ^+ and compare our results to the present SAPHIR data [2]. The value of κ_Θ is still elusive, although there are some theoretical suggestions on this quantity [9, 13]. We consider it as a parameter and vary its value between $-0.7 \leq \kappa_\Theta \leq 0.7$.

The results are given in Fig. 2, where the cross sections are obtained by using the subtraction function and form factors of Eqs.(6) and (7) to reduce the strength of the Born terms. In relation with these functions we present the sensitivity of the cross sections to the cutoff parameter Λ by taking both $\Lambda = 1.8$ GeV [41, 44] and a somewhat lower value $\Lambda = 1.2$ GeV for comparison. Given the coupling constant $g_{KN\Theta} = 2.2$ with $\kappa_\Theta = 0$, the dotted lines with $\Lambda = 1.2$ GeV lower the

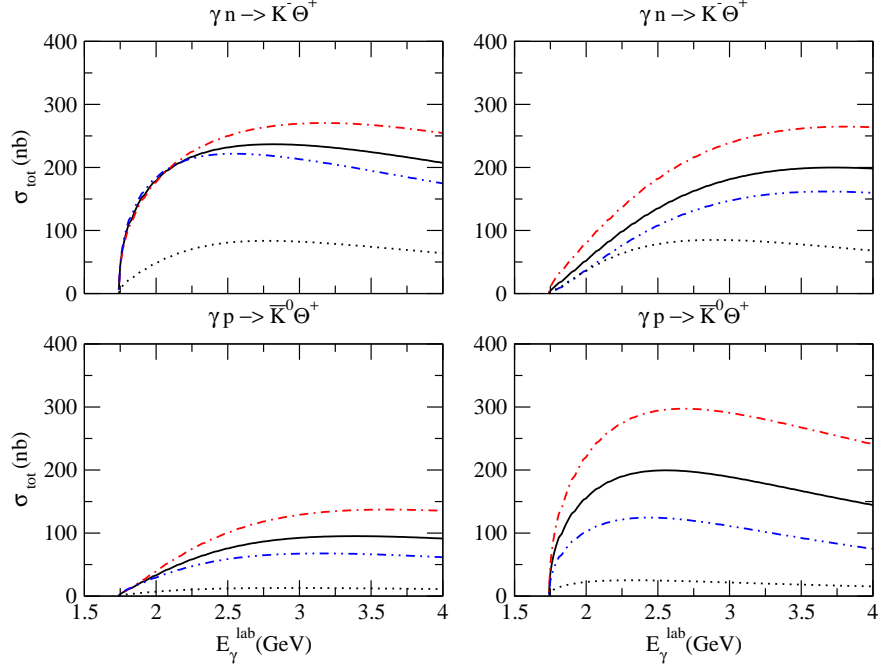


FIG. 2: Cross sections for $\gamma n \rightarrow K^- \Theta^+$ and for $\gamma p \rightarrow \bar{K}^0 \Theta^+$ when the Θ^+ has positive parity. The PV coupling scheme is displayed in the left column and the PS scheme is in the right column. Given the coupling constant $g_{KN\Theta} = 2.2$, dependence of the cross sections with $\Lambda = 1.8$ GeV and 1.2 GeV are shown. The dotted lines are the results of the Born amplitude with $\kappa_\Theta = 0$ and cutoff $\Lambda = 1.2$ GeV. The solid lines are the results of the Born amplitude with $\kappa_\Theta = 0$ and cutoff $\Lambda = 1.8$ GeV. The dot-dashed lines are the Born contributions with $\kappa_\Theta = 0.7$ and $\Lambda = 1.8$ GeV. The dot-dot-dashed lines with $\kappa_\Theta = -0.7$ and $\Lambda = 1.8$ GeV.

cross section down by more than one third of its magnitude as compared to the solid lines with $\Lambda = 1.8$ GeV in Fig. 2. As indicated in Refs. [44, 45], it probably makes more sense to consider the product $g_{KN\Theta} F_i(x)$ as the effective coupling strength but not the bare coupling constant $g_{KN\Theta}$ alone when form factors are incorporated. For instance, the effective coupling strength becomes $g_{KN\Theta} F_1(s) \simeq 0.36$ at threshold if $\Lambda = 1.2$ GeV. The smaller the cutoff Λ is, the more significantly \hat{F} is attenuated by the reductions in each form factor F_i as shown in Fig. 3. However, such a significant fall-off in \hat{F} may not be so desirable in order to minimize the ambiguity from the form factors. In Fig. 3, \hat{F} is very close to 1 near threshold almost independent of the scattering angle θ if $\Lambda = 1.8$ GeV. For this reason, we take the $\Lambda = 1.8$ GeV in what follows.

In Fig. 2, the cross section for $\gamma n \rightarrow K^- \Theta^+$ is about 150 nb in the PS and 250 nb in the PV scheme near $E_\gamma = 2.5$ GeV. The cross section for $\gamma p \rightarrow \bar{K}^0 \Theta^+$ is about 200 nb in PS and 80 nb in the PV scheme. These results are from the Born contributions only and this point is in sharp contrast to the results of previous calculations. In Ref. [39], with more contributions of the two

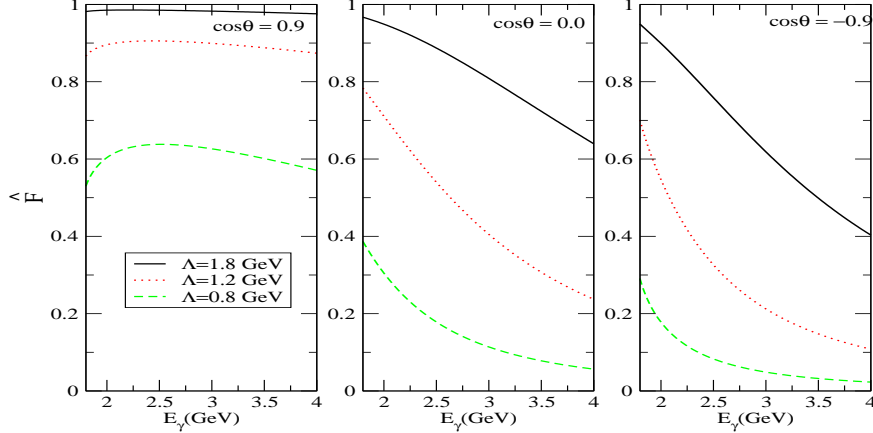


FIG. 3: Energy and angle dependence of the subtraction function \hat{F} for $\gamma p \rightarrow \bar{K}^0 \Theta^+$. The functional form of \hat{F} is given by Eq.(6). The solid line is for $\Lambda = 1.8$ GeV. The dotted line and the dashed line are for $\Lambda = 1.2$ GeV and 0.8 GeV respectively. Note that $\hat{F} = 1$ at $E_\gamma = 0$ below the threshold of the reaction regardless of Λ values.

and three body final state interactions considered, the authors used the t-channel and u-channel Born terms to obtain cross sections with the magnitude of 38 nb for $\gamma p \rightarrow \bar{K}^0 \Theta^+$ and of 280 nb for $\gamma n \rightarrow K^- \Theta^+$ in the PS scheme. Also in Ref. [41], the authors included K^* exchange in their PS coupling Born amplitude to obtain the cross sections about 320 ~ 400 nb for $\gamma p \rightarrow \bar{K}^0 \Theta^+$ and about 200 ~ 230 nb for $\gamma n \rightarrow K^- \Theta^+$, depending on the sign of $g_{K^* N \Theta}$. But the Born contributions to these total cross sections are found to be about 40 nb and 80 nb for each process and almost the rest of the cross sections are from K^* contributions. In fact their Born contributions up to $E_\gamma = 4$ GeV are smaller by a factor of $\frac{1}{3}$ or $\frac{1}{4}$ than our result in PS scheme of Fig. 2, despite the same cutoff Λ with ours. As a consequence, the K^* contributions relative to the Born terms in the cross sections are much larger than ours. Furthermore, in contrast to their findings in the κ_Θ contributions, our cross sections are significantly dependent on the variation of κ_Θ in case of PS coupling scheme, albeit parameterized as the same value with Ref. [41]. Besides the different type of form factor used in Ref. [39] from ours and Ref. [41], the apparent distinctions between these previous results and ours are mainly due to the different gauge prescriptions adopted in each model calculation. Although neither of the procedures adopted in Refs. [39, 41] violates the gauge invariance, we emphasize that they certainly need further improvement in going beyond just taking a single overall form factor from a field theoretic point of view. In Fig. 2, it is instructive to note that the cross section of $\gamma n \rightarrow K^- \Theta^+$ near threshold is similar to that of $\gamma n \rightarrow \pi^- p$ and also that of $\gamma p \rightarrow \bar{K}^0 \Theta^+$ to $\gamma p \rightarrow \pi^0 p$, since the two channels of Θ^+ production have the same charge exchange

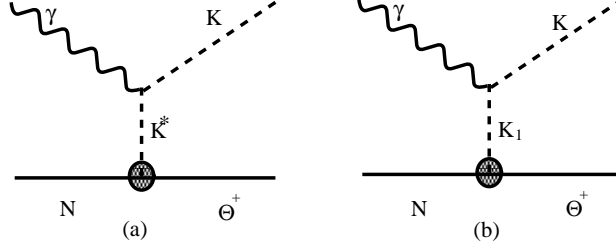


FIG. 4: Diagrams for t-channel K^* and K_1 exchanges in the $\gamma N \rightarrow K\Theta^+$ process.

structure of the Born terms with the corresponding two processes in the pion photoproduction. According to the results of Refs. [55, 56] where the couplings of the baryon octet with the anti-decuplet are analyzed, the Θ^+ is difficult to couple to any would-be nucleon resonances. We, thus, refer a qualitative analysis of our cross sections to those of the pion photoproduction near threshold where no significant contributions are attributed to the resonances [57]. With these in mind, the "nose" structure of PV coupling scheme of $\gamma n \rightarrow K^-\Theta^+$ near threshold is understood by the Kroll-Ruderman term and possibly the kaon pole term. The Kroll-Ruderman term dictates the threshold amplitude, giving large s-wave contribution to yield a rapid increase of cross section together with the kaon pole term. For the process $\gamma p \rightarrow \bar{K}^0\Theta^+$, there is neither Kroll-Ruderman term nor kaon pole term due to the charge conservation. Therefore, the cross section of the latter process is suppressed near threshold similar to the case of $\gamma p \rightarrow \pi^0 p$ [58, 59]. These qualitative features are apparent in the PV coupling scheme and consistent with the remark in Ref. [60] that the photoexcitation of the baryon anti-decuplet is strongly suppressed in the proton target and the process occurs mostly in the neutron target.

We now consider the contributions of t-channel vector meson K^* and K_1 axial vector meson exchanges. Fig. 4 depicts the Feynman diagrams for the K^* and K_1 exchanges in the t-channel. For the $K^*(890)(J^P = 1^-)$ exchange, we use the Lagrangians

$$\begin{aligned}\mathcal{L}_{K^*N\Theta} &= g_{K^*N\Theta} \bar{\Theta} \left(\gamma^\mu + \frac{\kappa^*}{M + M_\Theta} \sigma^{\nu\mu} \partial_\nu \right) K_\mu^{*\dagger} N + \text{h.c.}, \\ \mathcal{L}_{K^*K\gamma} &= \frac{g_{K^*K\gamma}}{m} \epsilon_{\alpha\beta\mu\nu} \partial^\alpha A^\beta \partial^\mu K^\dagger K^{*\nu} + \text{h.c.},\end{aligned}\quad (10)$$

where $g_{K^*N\Theta}$ and κ^* are respectively the vector coupling constant and the tensor coupling ratio of $K^*N\Theta$ vertex. Here m is a parameter of mass dimension for the anomalous coupling of $g_{K^*K\gamma}$. The transition amplitude for K^* exchange in the t-channel can be written as

$$\mathcal{M}_{K^*} = -G_{K^*N\Theta} \bar{u}_\Theta \left\{ \epsilon_{\alpha\beta\tau\sigma} k^\alpha \epsilon^\beta q^\tau \frac{(-g^{\sigma\mu} + q'^\sigma q'^\mu / M_{K^*}^2)}{t - M_{K^*}^2 + i\Gamma M_{K^*}} \left(\gamma_\mu + i \frac{\kappa^*}{M + M_\Theta} \sigma_{\nu\mu} q'^\nu \right) \right\} u_N, \quad (11)$$

with $G_{K^*N\Theta} = g_{K^*N\Theta} g_{K^*K\gamma} F_3(t) m^{-1}$, and $q'_\mu = (q - k)_\mu$. Including these contributions, we use

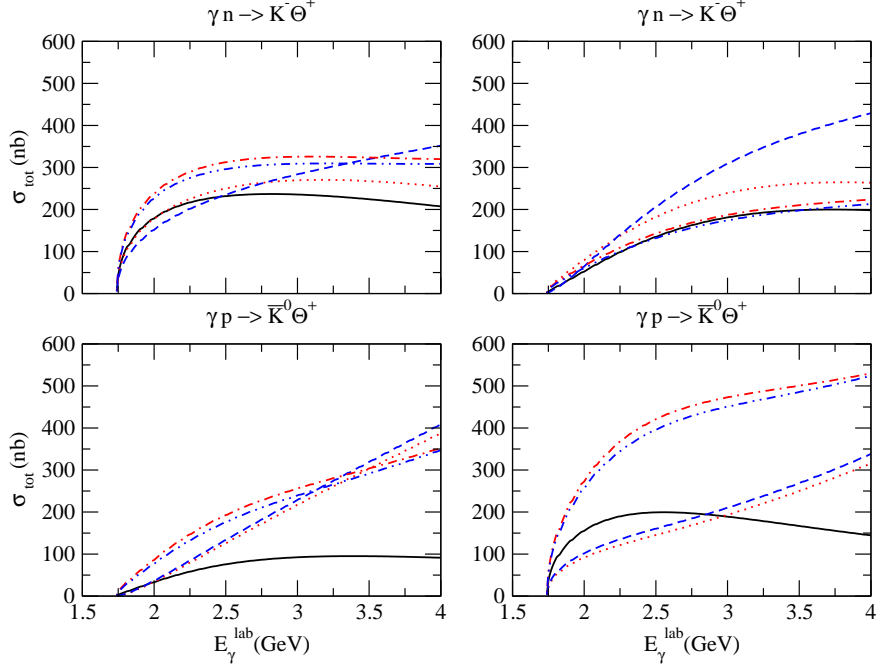


FIG. 5: Cross sections for $\gamma n \rightarrow K^- \Theta^+$ of PV(upper left) and PS scheme(upper right). Cross sections for $\gamma p \rightarrow \bar{K}^0 \Theta^+$ of PV(lower left) and PS scheme(lower right) when the Θ^+ has positive-parity. $\kappa_\Theta = 0$ in any cases for all panels. The solid lines are the contributions of the Born amplitude with $g_{K^*N\Theta} = 0$. The dotted lines are the sum of the Born terms and K^* with $g_{K^*N\Theta} = 1.32$. The dot-dashed lines the sum of the Born terms and K^* with $g_{K^*N\Theta} = -1.32$. The dashed lines are the sum in total of the Born terms, K^* and K_1 with $g_{K^*N\Theta} = 1.32$, $g_{K_1N\Theta} = -0.07$ for $\gamma n \rightarrow K^- \Theta^+$ and $g_{K_1N\Theta} = -0.1$ for $\gamma p \rightarrow \bar{K}^0 \Theta^+$ respectively. The dot-dot-dashed lines are the sum in total of the Born terms, K^* and K_1 with $g_{K^*N\Theta} = -1.32$, $g_{K_1N\Theta} = +0.07$ for $\gamma n \rightarrow K^- \Theta^+$ and $g_{K_1N\Theta} = +0.1$ for $\gamma p \rightarrow \bar{K}^0 \Theta^+$ respectively.

$g_{K^*K^\pm\gamma} = 0.254$ for the charged kaon anomalous decay and $g_{K^*K^0\gamma} = 0.388$ for the neutral kaon decay that are cited in PDG [61]. Following Ref. [40], the unknown coupling $g_{K^*N\Theta}$ was deduced to be 1.32 from the assumption, $g_{K^*N\Theta}/g_{KN\Theta} = 0.6$. We adopt this value of $g_{K^*N\Theta}$ and do not consider the tensor coupling contributions of both K^* and K_1 to avoid any further parameters. The interaction Lagrangians for the axial vector meson $K_1(1270)(J^P = 1^+)$ coupling to $K_1N\Theta^+$ and $K_1K\gamma$ are given by

$$\begin{aligned} \mathcal{L}_{K_1N\Theta} &= g_{K_1N\Theta} \bar{\Theta} \left(\gamma_\mu + \frac{\kappa_1}{M + M_\Theta} \sigma_{\nu\mu} \partial^\nu \right) K_1^{\mu\dagger} \gamma_5 N + \text{h.c.}, \\ \mathcal{L}_{K_1K\gamma} &= -i \frac{g_{K_1K\gamma}}{m} K^\dagger (\partial_\mu A_\nu \partial^\mu K_1^\nu - \partial_\mu A_\nu \partial^\nu K_1^\mu) + \text{h.c.}, \end{aligned} \quad (12)$$

where $g_{K_1N\Theta}$ and κ_1 are the axial vector coupling constant and the tensor coupling ratio of $K_1N\Theta$

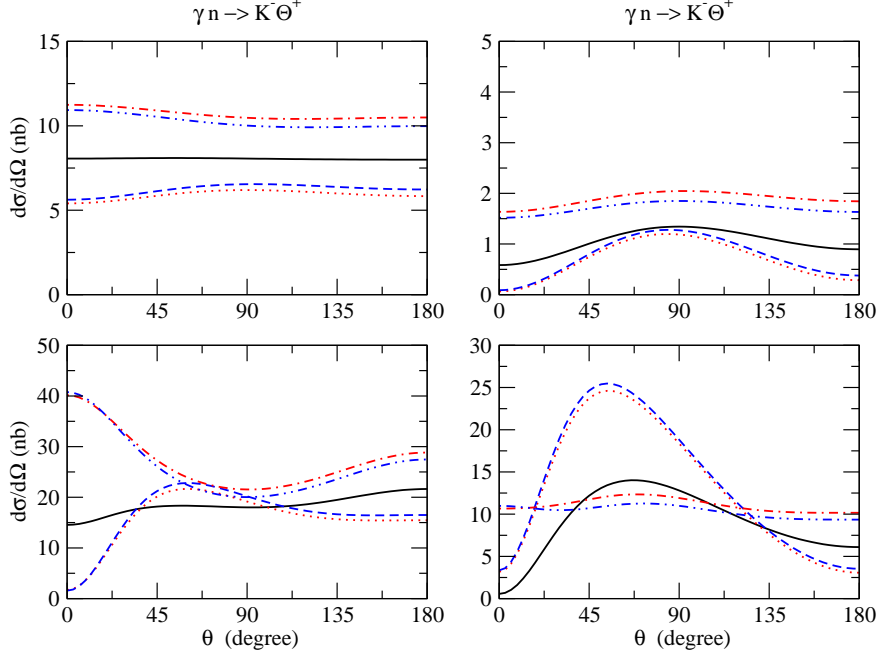


FIG. 6: Angular distributions for $\gamma n \rightarrow K^- \Theta^+$ at $E_\gamma = 1.8$ GeV(upper left), $E_\gamma = 2.5$ GeV(lower left) of PV and $E_\gamma = 1.8$ GeV(upper right), $E_\gamma = 2.5$ GeV(lower right) of PS scheme when the parity of Θ^+ is positive. The notations are the same as in Fig. 5

vertex, respectively. Then, the transition amplitude for the t-channel K_1 exchange is given by,

$$\mathcal{M}_{K_1} = G_{K_1 N \Theta} \bar{u}_\Theta(k \cdot q' \epsilon_\mu - \epsilon \cdot q' k_\mu) \frac{(-g^{\mu\nu} + q'^\mu q'^\nu / M_{K_1}^2)}{t - M_{K_1}^2 + i\Gamma M_{K_1}} \left(\gamma_\nu + i \frac{\kappa_1}{M + M_\Theta} \sigma_{\alpha\nu} q'^\alpha \right) \gamma_5 u_N, \quad (13)$$

with $G_{K_1 N \Theta} = g_{K_1 N \Theta} g_{K_1 K \gamma} F_3(t) m^{-1}$. For the axial vector meson coupling constant $g_{K_1 K \gamma}$, there are no empirical data available for the decay $K_1 \rightarrow K \gamma$ except for its decay channel to ρ meson via the process $K_1 \rightarrow \rho K$ [61]. In Ref. [62], by using the effective Lagrangian given by Eq.(12) for the interaction vertex $K_1 K \rho$, the decay width $\Gamma_{K_1 \rightarrow K \rho}$ was estimated to be 37.8 MeV and the coupling constant $g_{K_1 K \rho}$ was determined to be 12.0. Using this value for $g_{K_1 K \rho}$, we deduce the coupling constant $g_{K_1 K \gamma} = 0.6$ by applying the vector dominance relation for $g_{K_1 K \gamma} = \frac{e}{f_\rho} g_{K_1 K \rho}$, where $f_\rho^2/4\pi = 2.9$. In order to determine the axial vector coupling constant $g_{K_1 N \Theta}$, we make use of the ratio $g_{K^* K \gamma} g_{K^* p \Lambda} / g_{K_1 K \gamma} g_{K_1 p \Lambda} \simeq -8.6$, which is extracted from WJC model for $K^+ \Lambda$ electromagnetic production [63] and assume that this ratio is valid also for $g_{K^* K \gamma} g_{K^* N \Theta} / g_{K_1 K \gamma} g_{K_1 N \Theta}$. Then, we obtain $g_{K_1 N \Theta} = -0.07$ for $\gamma n \rightarrow K^- \Theta^+$ and $g_{K_1 N \Theta} = -0.1$ for $\gamma p \rightarrow \bar{K}^0 \Theta^+$, respectively.

In Fig. 5, we present the results of K^* and K_1 contributions to the cross sections of $\gamma n \rightarrow K^- \Theta^+$ and $\gamma p \rightarrow \bar{K}^0 \Theta^+$ in both coupling schemes. In most cases, K^* gives significant contributions, whereas the role of K_1 is minor and these vector mesons give contributions to $\gamma p \rightarrow \bar{K}^0 \Theta^+$ larger than $\gamma n \rightarrow K^- \Theta^+$. In this figure, the results of these contributions are more favorable when

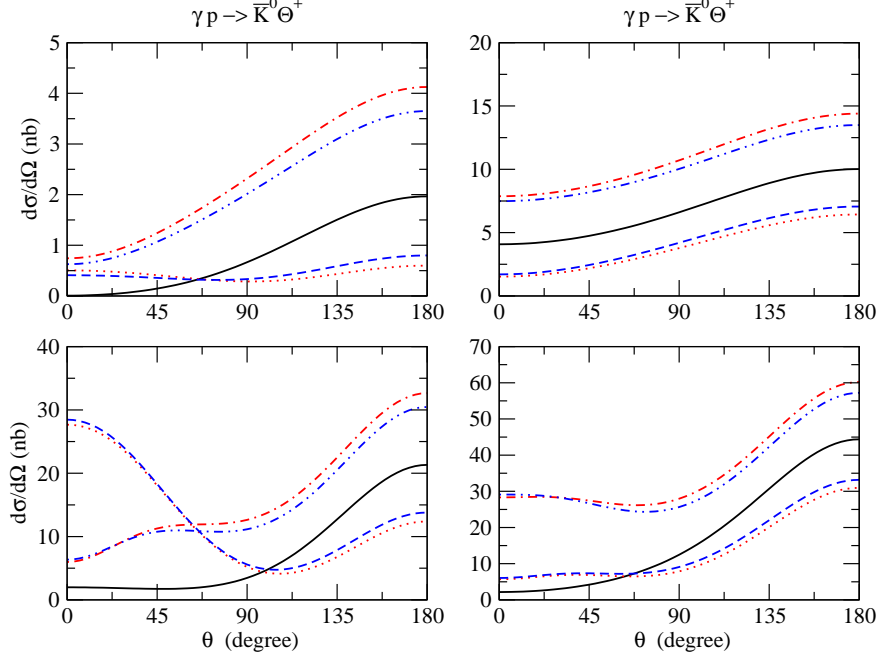


FIG. 7: Angular distributions for $\gamma p \rightarrow \bar{K}^0 \Theta^+$ at $E_\gamma = 1.8$ GeV (upper left), $E_\gamma = 2.5$ GeV (lower left) of PV and $E_\gamma = 1.8$ GeV (upper right), $E_\gamma = 2.5$ GeV (lower right) of PS scheme when the parity of Θ^+ is positive. The notations are the same as in Fig. 5

$g_{K^*N\Theta} = 1.32$, $g_{K_1N\Theta} = -0.07(-0.1)$ for $\gamma n \rightarrow K^- \Theta^+$ ($\gamma p \rightarrow \bar{K}^0 \Theta^+$) as depicted by the dashed lines. They give the same order of magnitude to the cross sections for each process at $E_\gamma = 2.5$ GeV, regardless of the coupling scheme. Around this energy, the dashed lines of the cross section for $\gamma n \rightarrow K^- \Theta^+$ are about 230 nb, and for $\gamma p \rightarrow \bar{K}^0 \Theta^+$ about 150 nb, respectively.

In Fig. 6, the differential cross sections for $\gamma n \rightarrow K^- \Theta^+$ are displayed near threshold $E_\gamma = 1.8$ GeV and at $E_\gamma = 2.5$ GeV. It is interesting to see that the angular distributions of the kaon produced near threshold, $E_\gamma = 1.8$ GeV, are isotropic both in the PV and PS schemes. These are due to the s-wave dominance from the Kroll-Ruderman term in the case of PV, and from the s-channel nucleon pole term in the case of PS, respectively. Notice that the scales of the cross sections in the two schemes are different. This feature of the s-wave production near threshold can be anticipated from the parity and angular momentum conservation which states that the angular momentum of the produced kaon is in the s-wave state near threshold, if the parity of the Θ^+ is positive. In the energy bin $E_\gamma = 2.5$ GeV, the interference of K^* and K_1 exchanges develops a peak around $\theta = 45^\circ$ in both coupling schemes when $g_{K^*N\Theta} = 1.32$, $g_{K_1N\Theta} = -0.07$ as depicted by the dashed lines.

In Fig. 7, the angular distributions of $\gamma p \rightarrow \bar{K}^0 \Theta^+$ are presented. There appear small deviations

from the isotropic angular distribution in the Born contribution and the backward asymmetries are observed near threshold. These backward enhancements hold even at $E_\gamma = 2.5$ GeV both in the PV and PS schemes. They are resulting from the u-channel contribution of the Born terms, since there is no kaon pole term in this process. At $E_\gamma = 2.5$ GeV, the change in the sign of K^* and K_1 coupling constants in the PV coupling scheme shifts the position of a peak from the the very forward angle for $g_{K^*N\Theta} = 1.32$, $g_{K_1N\Theta} = -0.1$ to the very backward angle for $g_{K^*N\Theta} = -1.32$, $g_{K_1N\Theta} = 0.1$. It is worth noting that the threshold behaviors of the Born terms of these two processes given in Figs. 5, 6 and 7 show a close similarity to those of $\gamma n \rightarrow \pi^- p$ and $\gamma p \rightarrow \pi^0 p$ near threshold found in Refs. [58, 59], as mentioned before.

III. PHOTOPRODUCTION FOR THE NEGATIVE PARITY Θ^+

We now turn to the case of Θ^+ photoproduction when it has the negative parity. The electromagnetic coupling vertex of the negative parity Θ^+ baryon is given by,

$$\mathcal{L}_{\gamma\Theta\Theta} = -\bar{\Theta}\gamma_5 \left[Q_\Theta\gamma^\mu - \frac{\kappa_\Theta}{2M_\Theta}\sigma_{\mu\nu}\partial^\nu \right] \gamma_5\Theta A^\mu. \quad (14)$$

The interaction Lagrangians of the negative parity Θ^+ for the PS and PV couplings are of the forms;

$$\begin{aligned} \mathcal{L}_{KN\Theta}^{PS} &= -ig_{KN\Theta}\bar{\Theta}NK, \\ \mathcal{L}_{KN\Theta}^{PV} &= -\frac{g_{KN\Theta}}{M-M_\Theta}\bar{\Theta}\gamma^\mu N\partial_\mu K, \end{aligned} \quad (15)$$

which are equivalent to each other for the free baryons. It must be noted, however, that they are slightly different from each other when, reduced to the non-relativistic spinor forms at threshold, i.e.,

$$\begin{aligned} \mathcal{L}_{KN\Theta}^{PS} &= -ig_{KN\Theta}\chi_\Theta^\dagger\chi_N K + \dots, \\ \mathcal{L}_{KN\Theta}^{PV} &= -ig_{KN\Theta}\frac{m_K}{M-M_\Theta}\chi_\Theta^\dagger\chi_N K + \dots. \end{aligned} \quad (16)$$

The difference is by the factor $\frac{m_K}{M-M_\Theta} \simeq 0.85$, which makes the PV coupling version somewhat smaller than the PS one by the factor of 0.85. The Born amplitude for the negative parity Θ^+ photoproduction can be derived by using the Lagrangians in Eqs.(14) and (15) for the coupling vertices relevant to the interaction diagrams shown in Fig. 1. This leads to the replacement of the final state $\bar{u}_\Theta \rightarrow -\bar{u}_\Theta\gamma_5$ at every $KN\Theta$ vertex and the u-channel propagator of Θ^+ , $S_F(p' - k) \rightarrow -\gamma_5 S_F(p' - k)\gamma_5$ in the amplitude given by Eq.(1), i.e.,

$$\mathcal{M}_{Born} = \mathcal{M}_{PV-pole} + \mathcal{M}_{KR} + \mathcal{M}_c, \quad (17)$$

where

$$\begin{aligned}
& \mathcal{M}_{PV-pole} \\
&= \frac{eg_{KN\Theta}}{M - M_\Theta} \bar{u}_\Theta(p') \left\{ -F_1(s) \not{q} \frac{(\not{p}' + \not{k} + M)}{s - M^2} [Q_N \not{\epsilon} + i \frac{\kappa_N}{2M} \sigma^{\mu\nu} \epsilon_\mu k_\nu] + [-Q_\Theta \not{\epsilon} + i \frac{\kappa_\Theta}{2M_\Theta} \sigma^{\mu\nu} \epsilon_\mu k_\nu] \right. \\
&\quad \left. \times \frac{(\not{p}' - \not{k} + M_\Theta)}{u - M_\Theta^2} \not{q} F_2(u) - Q_K F_3(t) \frac{(M - M_\Theta)(2q - k) \cdot \epsilon}{t - m_K^2} \right\} u_N(p), \tag{18}
\end{aligned}$$

$$\mathcal{M}_{KR} = \frac{eg_{KN\Theta}}{M - M_\Theta} \bar{u}_\Theta(p') \left\{ F_1(s) Q_N - Q_\Theta F_2(u) \right\} \not{\epsilon} u_N(p), \tag{19}$$

$$\begin{aligned}
\mathcal{M}_c &= eg_{KN\Theta} \bar{u}_\Theta(p') \left\{ (F_1(s) - \widehat{F}) Q_N \frac{(2p + k) \cdot \epsilon}{s - M^2} + Q_\Theta (F_2(u) - \widehat{F}) \frac{(2p' - k) \cdot \epsilon}{u - M_\Theta^2} \right. \\
&\quad \left. + Q_K (F_3(t) - \widehat{F}) \frac{(2q - k) \cdot \epsilon}{t - m_K^2} \right\} u_N(p). \tag{20}
\end{aligned}$$

By the similar procedure, the PS coupling Born amplitude is given by,

$$\mathcal{M}_{Born} = \mathcal{M}_{PS-pole} + \mathcal{M}_c, \tag{21}$$

where the contact interaction term \mathcal{M}_c is given by the same equation, Eq.(20), and

$$\begin{aligned}
& \mathcal{M}_{PS-pole} \\
&= eg_{KN\Theta} \bar{u}_\Theta(p') \left\{ -F_1(s) \frac{(\not{p}' + \not{k} + M)}{s - M^2} [Q_N \not{\epsilon} + i \frac{\kappa_N}{2M} \sigma^{\mu\nu} \epsilon_\mu k_\nu] + [-Q_\Theta \not{\epsilon} + i \frac{\kappa_\Theta}{2M_\Theta} \sigma^{\mu\nu} \epsilon_\mu k_\nu] \right. \\
&\quad \left. \times \frac{(\not{p}' - \not{k} + M_\Theta)}{u - M_\Theta^2} F_2(u) - Q_K F_3(t) \frac{(2q - k) \cdot \epsilon}{t - m_K^2} \right\} u_N(p). \tag{22}
\end{aligned}$$

For an application of the K^* and K_1 exchanges in the t-channel, we use the transition amplitudes of the positive parity Θ^+ cases, i.e. Eqs.(11) and (13), replacing \bar{u}_Θ by $-\bar{u}_\Theta \gamma_5$ in the $K^*N\Theta$ and $K_1N\Theta$ vertices.

The process for the negative parity Θ^+ production was considered in Refs. [38, 40, 41, 42] and found to have smaller cross section than the positive-parity Θ^+ production. In Fig. 8, the total cross sections are shown for both processes with $g_{KN\Theta} = 0.3$ taken from the decay width $\Gamma_\Theta \simeq 5$ MeV. For the K^* and K_1 coupling constants, we use $g_{K^*N\Theta} = 0.18$, keeping the ratio $g_{K^*N\Theta}/g_{KN\Theta} = 0.6$. The coupling constant $g_{K_1N\Theta}$ is determined from the assumption that the ratio $g_{K^*K\gamma}g_{K^*p\Lambda(1405)}/g_{K_1K\gamma}g_{K_1p\Lambda(1405)} = -0.7$ extracted from Ref. [63] holds for the present coupling ratio $g_{K^*K\gamma}g_{K^*N\Theta}/g_{K_1K\gamma}g_{K_1N\Theta}$ as well. In the figures, the role of K_1 is appreciable in the negative parity Θ^+ and the cross sections are sensitive to the sign of K^* and K_1 coupling constants. This is analogous to the K^* dominance in the positive parity production, since the parities of K^* and K_1 are opposite to each other. Depending on the signs of the K^* and K_1

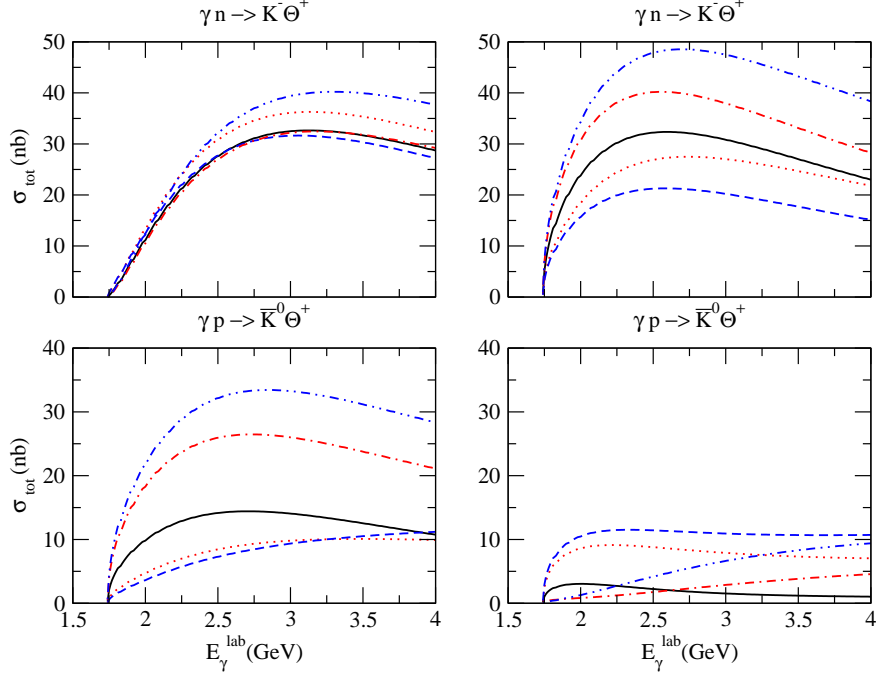


FIG. 8: Cross sections for $\gamma n \rightarrow K^- \Theta^+$ of PV (upper left) and PS scheme (upper right). Cross sections for $\gamma p \rightarrow \bar{K}^0 \Theta^+$ of PV (lower left) and PS scheme (lower right) when the Θ^+ has negative parity. $\kappa_\Theta = 0$ in all cases for all panels. The solid lines are the contribution of the Born amplitude with $g_{K N \Theta} = 0.3$, $g_{K^* N \Theta} = 0$. The dotted lines are the sum of the Born amplitude and K^* with $g_{K^* N \Theta} = 0.18$. The dot-dashed lines are the sum of the Born amplitude and K^* with $g_{K^* N \Theta} = -0.18$. The dashed lines are the sum in total of the Born terms, K^* and K_1 with $g_{K^* N \Theta} = 0.18$, $g_{K_1 N \Theta} = -0.1$ for $\gamma n \rightarrow K^- \Theta^+$ and $g_{K_1 N \Theta} = -0.16$ for $\gamma p \rightarrow \bar{K}^0 \Theta^+$ respectively. The dot-dot-dashed lines are the sum in total of the Born, K^* and K_1 with $g_{K^* N \Theta} = -0.18$, $g_{K_1 N \Theta} = +0.1$ for $\gamma n \rightarrow K^- \Theta^+$ and $g_{K_1 N \Theta} = +0.16$ for $\gamma p \rightarrow \bar{K}^0 \Theta^+$ respectively.

coupling constants, the cross sections for $\gamma n \rightarrow K^- \Theta^+$ are around 30 nb for PV, and 20 ~ 50 nb for PS schemes at $E_\gamma = 2.5$ GeV respectively. While for $\gamma p \rightarrow \bar{K}^0 \Theta^+$, the cross sections are about 7 ~ 33 nb in the PV, and 2 ~ 12 nb in the PS schemes. From these figures we find that the reaction $\gamma n \rightarrow K^- \Theta^+$ is still dominant over the reaction $\gamma p \rightarrow \bar{K}^0 \Theta^+$ in the case of the negative parity Θ^+ as well. It should be noted that the inclusion of magnetic moment κ_Θ could give an additional contribution to the cross sections.

In comparison with the cross sections of the positive parity Θ^+ production in Fig. 5, the cross sections in the case of negative parity are suppressed roughly by an order of magnitude. This is consistent with the previous calculations presented in Refs. [39, 41]. The reason for the suppression is mainly because the adopted coupling constant $g_{K N \Theta} = 0.3$ taken from $\Gamma_\Theta \simeq 5$ MeV is smaller by a factor of $\frac{1}{7}$ than that of positive parity. This reduction is of course reflected in the suppression of

cross sections roughly by an order of magnitude smaller than the existing SAPHIR experimental cross section. Thus, if we trust the existing SAPHIR data, then we may well doubt the possibility of negative parity state of Θ^+ . However, there exists a rather large uncertainty in the present measurement of the decay width of the Θ^+ . Also, as we demonstrated in the positive parity case, the cross sections calculated in the framework of hadron models are largely dependent on the gauge prescription as well as the cutoff Λ . Moreover, let us consider the decay width of the transition, $\Theta^+(\frac{1}{2}^\pm) \rightarrow KN(\frac{1}{2}^+)$ with both parities retained; i.e.,

$$\Gamma_{\Theta(\frac{1}{2}^\pm)} = \frac{g_{KN\Theta}^2}{2\pi} \frac{|\mathbf{q}|}{M_\Theta} (\sqrt{M^2 + |\mathbf{q}|^2} \mp M), \quad (23)$$

and suppose that the coupling constant $g_{KN\Theta}$ is *a priori* given and the kaon momentum $|\mathbf{q}|$ in the Θ^+ rest frame is small. Then, the Eq.(23) implies that the width Γ_Θ near threshold would be small for the positive parity Θ^+ by the subtraction of nucleon mass from its energy, and vice versa for the negative parity. This means that the decay of the positive parity is kinematically forbidden for small momentum and initially a negative parity state of Θ^+ is more likely to decay to the final nucleon and kaon. In this respect, analyzing only the total cross sections does not seem to provide a decisive conclusion on the parity of the Θ^+ . We thus analyze further these processes by presenting the angular distributions.

The angular distributions for $\gamma n \rightarrow K^-\Theta^+$ and $\gamma p \rightarrow \bar{K}^0\Theta^+$ are displayed in Figs. 9 and 10, respectively. By the parity and angular momentum conservation, the produced kaon is anticipated to be in the p-wave state near threshold when the produced Θ^+ has negative parity. Such a feature is well reproduced in $\gamma n \rightarrow K^-\Theta^+$, whereas it is less clear for $\gamma p \rightarrow \bar{K}^0\Theta^+$, regardless of the coupling schemes of the $KN\Theta^+$ interaction. Note that the scales of the cross sections of $E_\gamma=1.8$ GeV in the two schemes are different in Fig. 9. In particular, at the photon energy $E_\gamma = 2.5$ GeV we observe a forward peak due to a coherent interference of the Born terms with K^* and K_1 right around 45° both in the two schemes in Fig. 9. The coherent peak of the Born terms around 45° is understood by the t-channel kaon pole dominance. In the case of $\gamma p \rightarrow \bar{K}^0\Theta^+$ presented in Fig. 10, the apparent flat curves of the Born contribution may be due to the small u-channel Born contribution weakened by the small coupling constant $g_{KN\Theta}$. Therefore, the development of the angular distribution of the cross section in this process comes from the t-channel K^* and K_1 contributions as the photon energy increases.

Before closing this section, it should be remarked that the angular distributions of $\gamma n \rightarrow K^-\Theta^+$ and $\gamma p \rightarrow \bar{K}^0\Theta^+$ near threshold in particular show a clear distinction between two opposite parities of the Θ^+ baryon and they are given in a rather model-independent way. As we have demonstrated

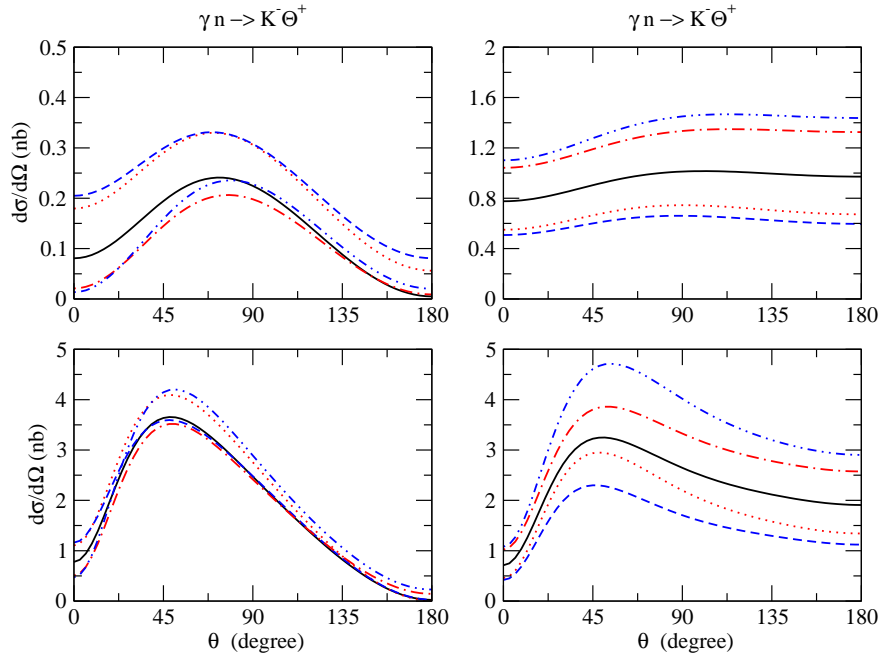


FIG. 9: Angular distributions for $\gamma n \rightarrow K^- \Theta^+$ at $E_\gamma = 1.8$ GeV (upper left), $E_\gamma = 2.5$ GeV (lower left) of PV and $E_\gamma = 1.8$ GeV (upper right), $E_\gamma = 2.5$ GeV (lower right) of PS scheme with the negative parity Θ^+ . The notations are the same as in Fig. 8

up to this point, near threshold where the orbital excitations of kaon other than $L = 0$ or 1 are suppressed, the conservation of parity and angular momentum imposes a specified form on the shape of angular distribution of $\gamma N \rightarrow K \Theta^+$, depending on what parity state of the Θ^+ is. Therefore, the observation of the reaction near threshold can provide an unambiguous way to clarify the parity of the Θ^+ . The importance of using this sort of conservation laws near threshold was also emphasized in Ref. [64], but for the different reaction $pp \rightarrow \Sigma^+ \Theta^+$. The reaction they suggested instead of the Θ^+ photoproduction takes the advantage of giving more tight condition on the parity and angular momentum at the initial pp state. However, the photoproduction of Θ^+ has already been observed and seems to be more available for the present experiment than the reaction suggested in Ref. [64].

IV. SUMMARY AND DISCUSSION

We investigated the possibility of using photon induced Θ^+ production, $\gamma n \rightarrow K^- \Theta^+$ and $\gamma p \rightarrow \bar{K}^0 \Theta^+$, to discriminate the parity of the Θ^+ baryon. The processes are calculated for two possible parity states of the Θ^+ baryon using the hadron model where the interaction of the $KN\Theta$ vertex is considered both in the PV and PS coupling schemes. We employ the broader basis of prescription for the gauge invariance based on the Ohta and Haberzettl methods, as discussed in

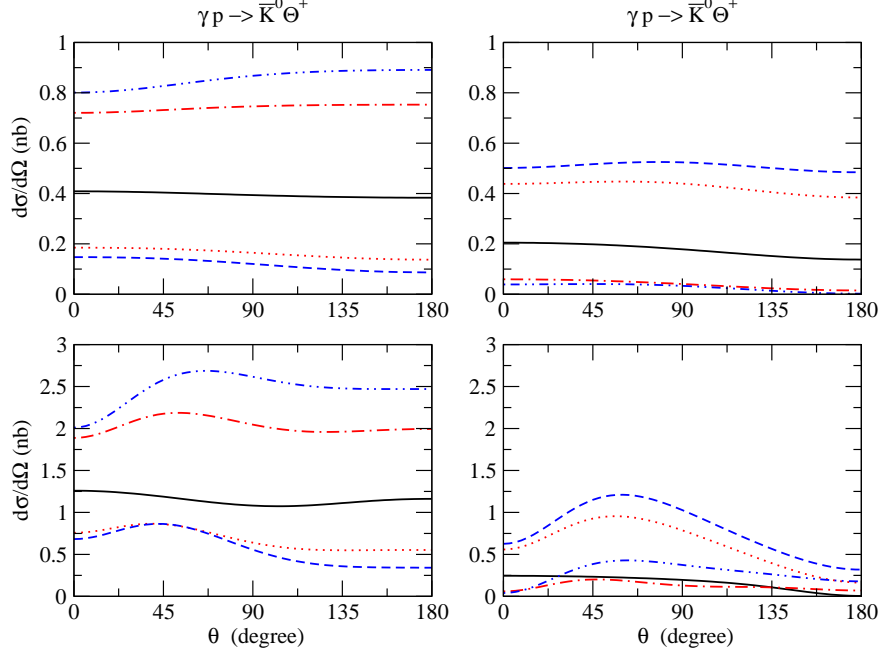


FIG. 10: Angular distributions for $\gamma p \rightarrow \bar{K}^0 \Theta^+$ at $E_\gamma = 1.8$ GeV(upper left), $E_\gamma = 2.5$ GeV(lower left) of PV and $E_\gamma = 1.8$ GeV(upper right), $E_\gamma = 2.5$ GeV(lower right) of PS scheme with the negative parity Θ^+ . The notations are the same as in Fig. 8

the study of $K^+\Lambda$ and $K^+\Sigma$ photoproductions [48, 49, 50]. The results for the total and differential cross sections are to a large extent different from those of previous calculations [38, 39, 41, 42], indicating that there is a wide theoretical uncertainty associated with the different assumptions on the gauge prescription. We may summarize the differences as follows. (i) With the decay width 5 MeV, the cross sections of the positive parity Θ^+ from the neutron and proton target are comparable to the present SAPHIR data, whereas the cross sections of the negative parity are found to be only tens of nb. Nevertheless, the uncertainty in the experimental data are now under discussion and if the cross sections are indeed an order of magnitude smaller, as presented in Refs. [54, 65], than the published SAPHIR data [2], then the results of the present work are likely to support the photoproduction by the negative parity Θ^+ even with the coupling constant $g_{KN\Theta} = 0.3$. Our results also show that the cross section of the Θ^+ production from the neutron is on the whole larger than that of Θ^+ production from the proton. (ii) Using the empirical ratio of $\frac{g_{K^*K\gamma}g_{K^*N\Lambda}}{g_{K_1K\gamma}g_{K_1N\Lambda}}$ extracted from $K^+\Lambda$ electromagnetic production for the determination of the coupling constants, $g_{K^*N\Theta}$ and $g_{K_1N\Theta}$, we obtain the K^* and K_1 contributions and find that the K^* contribution is in general important and K_1 contribution to the negative Θ^+ parity is not negligible either. However, these contributions are not so much dominant over the Born contribution as claimed in

Ref. [41]. This point is supported by the generally known fact that the contributions of vector meson $\rho(\omega)$ are about 10 % of the Born contributions at best to the threshold amplitudes of the reactions $\gamma n \rightarrow \pi^- p$ and $\gamma p \rightarrow \pi^0 p$ [57]. (iii) Finally, we find that the angular distributions of the production processes for the two opposite parity states are less dependent on the model parameters and distinct from each other. Therefore, we suggest that the observation of angular distribution in the photoproduction process can serve as a more useful tool to distinguish the parity of the Θ^+ baryon as compared to the measurement of total cross sections only.

Acknowledgments

This work was supported in part by 2003 Hankuk Aviation university Faculty Research Grant and in part by a grant from the U.S. Department of Energy (DE-FG02-96ER 40947).

-
- [1] LEPS Collaboration, T. Nakano *et al.*, Phys. Rev. Lett. **91**, 012002 (2003).
 - [2] SAPHIR Collaboration, J. Barth *et al.*, Phys. Lett. B **572**, 127 (2003); hep-ex/0307083.
 - [3] CLAS Collaboration I, S. Stepanyan *et al.*, Phys. Rev. Lett. **91**, 252001 (2003).
 - [4] CLAS Collaboration II, V. Kubarovsky *et al.*, Phys. Rev. Lett. **92**, 032001 (2004).
 - [5] HERMES Collaboration, A. Airapetian *et al.*, Phys. Lett. **B 585**, 213 (2004).
 - [6] V. V. Barmin *et al.* (DIANA Collaboration), Phys. Atom. Nucl. **66**, 1715 (2003).
 - [7] A. E. Asratyan, A. G. Dolgolenko, and M. A. Kubantsev, hep-ex/0309042.
 - [8] SVD Collaboration, A. Aleev *et al.*, hep-ex/0401024.
 - [9] D. Diakonov, V. Petrov, and M. Polyakov, Z. Phys. A **359**, 305 (1997).
 - [10] H. Weigel, Eur. Phys. J. A **2**, 391 (1998).
 - [11] M. Chemtob, Nucl. Phys. **B256**, 600 (1985).
 - [12] M. Praszalowicz, Phys. Lett. B **575**, 234 (2003).
 - [13] R. L. Jaffe and F. Wilczek, Phys. Rev. Lett. **91**, 232003 (2003).
 - [14] R. L. Jaffe, Phys. Rev. D **15**, 267 (1977); Phys. Rev. D **15**, 281 (1977).
 - [15] K. Cheung hep-ph/0308176.
 - [16] Fl. Stancu and D. O. Riska, Phys. Lett. B **575**, 242 (2003).
 - [17] C. E. Carlson, C. D. Carone, H. J. Kwee, and V. Nazaryan, Phys. Lett. B **573**, 101 (2003); Phys. Lett. B **579**, 52 (2004).
 - [18] L. Ya. Golzman, Phys. Lett. B **575**, 18 (2003); hep-ph/0309092.
 - [19] R. A. Williams and P. Guèye, nucl-th/0308058.
 - [20] M. karliner and H. J. Lipkin, Phys. Lett. B **575**, 249 (2003).

- [21] E. Shuryak and I. Zahed, hep-ph/0310270.
- [22] H. Walliser and V. B. Kopeliovich, J. Exp. Theor. Phys. **97**, 433 (2003).
- [23] B. K. Jennings and K. Maltman, hep-ph/0308286.
- [24] D. Borisyuk, M. Faber, and A. Kobushkin, hep-ph/0307370.
- [25] N. Itzhaki, I. R. Klebanov, P. Ouyang, and L. Rastelli, hep-ph/0309305.
- [26] B. Wu and B.-Q. Ma, hep-ph/0311331.
- [27] S.-L. Zhu, Phys. Rev. Lett. **91**, 232002 (2003).
- [28] R. D. Matheus, F. S. Navarra, M. Nielsen, R. da Silva, and S. H. Lee, Phys. Lett. B **578**, 323 (2004).
- [29] J. Sugiyama, T. Doi, and M. Oka, Phys. Lett. B **581**, 167 (2004).
- [30] A. Hosaka, Phys. Lett. B **571**, 55 (2003).
- [31] T. D. Cohen, Phys. Lett. B **581**, 175 (2004) ; T. D. Cohen and R. F. Lebed, Phys. Lett. B **578**, 150 (2004).
- [32] F. Csikor, Z. Fodor, S. D. Katz, and T. G. Kovács, hep-lat/0309090.
- [33] S. Sasaki, hep-lat/0310014.
- [34] B. G. Wybourne, hep-ph/0307170.
- [35] R. Bijker, M. M. Giannini, and E. Santopinto hep-ph/0310281.
- [36] J. Randrup, Phys. Rev. C **68**, 031903 (2003).
- [37] L. W. Chen, V. Greco, C. M. Ko, S. H. Lee, and W. Liu nucl-th/0308006.
- [38] S.-I. Nam, A. Hosaka, and H.-C. Kim, Phys. Lett. B **579**, 43 (2004).
- [39] W. Liu and C. M. Ko, Phys. Rev C **68**, 045203 (2003); nucl-th/0309023.
- [40] W. Liu and C. M. Ko, Phys. Rev. C **69**, 025202 (2004).
- [41] Y. S. Oh, H. C. Kim, and S.-H. Lee, Phys. Rev. D **69**, 014009 (2004).
- [42] Q. Zhao and J. S. Al-Khalili, hep-ph/0310350.
- [43] K. Nakayama and K. Tsushima, Phys. Lett. B **583**, 269 (2004).
- [44] S. Janssen, J. Ryckebusch, D. Debruyne, and T. Van Cauteren, Phys. Rev. C **66**, 035202 (2002); Phys. Rev. C **65**, 015201 (2001).
- [45] S. Janssen, J. Ryckebusch, W. Van Nespén, D. Debruyne, and T. Van Cauteren, Eur. Phys. J. A **9**, 115 (2000).
- [46] C. Bennhold, T. Mart, A. Waluyo, H. Haberzettl, G. Penner, T. Feuster, and U. Mosel, nucl-th/9901066.
- [47] T. Mart, S. Sumowidagdo, C. Bennhold, and H. Haberzettl, nucl-th/0002036.
- [48] K. Ohta, Phys. Rev. C **40**, 1335 (1989); Phys. Rev. C **46**, 2519 (1992).
- [49] H. Haberzettl, Phys. Rev. C **56**, 2041 (1997). H. Haberzettl *et al.*, nucl-th/9804051. H. Haberzettl, Phys. Rev. C **62**, 034605 (2000).
- [50] H. Haberzettl, C. Bennhold, T. Mart, and T. Feuster, Phys. Rev. C **58**, R40 (1998).
- [51] R. M. Davidson and R. Workman, Phys. Rev. C **63**, 025210 (2001); Phys. Rev. C **63**, 058201 (2001).
- [52] S. Nussinov, hep-ph/0307357.
- [53] R. A. Arndt, I. I. Strakovsky, and R. L. Workman, nucl-th/0311030.

- [54] F. E. Close and Q. Zhao, hep-ph/0403159.
- [55] Y. S. Oh, H. C. Kim, and S. H. Lee, hep-ph/0310117.
- [56] D. Diakonov and V. Petrov, hep-ph/0310212.
- [57] D. Drechsel and L. Tiator, J. Phys. G: Nucl. Part. Phys. **18**, 449 (1992).
- [58] O. Hanstein, D. Drechsel, and L. Tiator, nucl-th/9709067; Nucl. Phys. A **632**, 561 (1998).
- [59] M. Fuchs *et al.*, Phys. Lett. B **368**, 20 (1996).
- [60] M. V. Polyakov and A. Rathke, hep-ph/0303138; Eur. phys. J. A **18**, 691 (2003).
- [61] <http://pdg.lbl.gov/pdg.html>
- [62] K. Haglin, Phys. Rev. C **50**, 1688 (1994).
- [63] R. A. Williams, C.-R. Ji, and S. R. Cotanch, Phys. Rev. C **46**, 1617 (1992).
- [64] A. W. Thomas, K. Hicks, and A. Hosaka, hep-ph/0312083; Prog. Theor. Phys. **111**, 291 (2004).
- [65] S.-I. Nam, A. Hosaka, and H.-C. Kim, hep-ph/0403009;